PAPER • OPEN ACCESS

Streamer propagation along a profiled dielectric surface

View the article online for updates and enhancements.

Streamer propagation along a profiled dielectric surface

H K H Meyer[1,*] **, R Marskar**[1] **, H Gjemdal**[2,3] **and F Mauseth**[2]

[1] SINTEF Energy Research, Sem Sælands vei 11, 7034 Trondheim, Norway
[2] NTNU—Norwegian University of Science and Technology, Trondheim, Norway

E-mail: hans.meyer@sintef.no and robert.marskar@sintef.no

CrossMark

Abstract
We investigate the propagation of positive streamers along a profiled dielectric surface in air at atmospheric pressure. Results from experiments and two-dimensional planar low-temperature plasma fluid simulations are presented and analysed. The test object consists of a disk-shaped high voltage electrode and a dielectric slab with 0.5 mm deep corrugations. The corrugated surface has a 47% larger surface area than the smooth reference surface. The experiments and simulations are performed at voltage levels that lead to either gap-bridging or arrested streamers. In both experiments and simulations, the streamers take a longer time to reach the ground electrode when propagating along the profiled surface than along the smooth reference surface. Also, arrested streamers stop closer to the high voltage electrode when a profiled surface is used. Streamers propagate closely along the surface profile in the simulations, which suggests that the observed surface profile effect is mainly a result of elongated streamer channels. Compared to the streamers propagating along the smooth surface, the elongated streamers on the profiled surface have less residual voltage at the streamer front to drive the streamer advancement.

(Some figures may appear in colour only in the online journal)

1. Introduction

1.1. Streamers

Streamers are low-temperature filamentary plasmas. They are precursors to lightning, arcs, and sparks, and exist naturally in the upper atmosphere as sprite discharges [1]. They are used in diverse fields such as gas sterilisation [2, 3], CO_2 conversion [4], aerodynamic flow control [5–7], and plasma catalysis [8–10]. They are characterised by filamentary growth in the form of irregular tree structures with self-enhanced fields at their tips.

In gases, streamers advance through electron impact ionisation in the streamer head. The ionisation process leaves behind electron–ion pairs that are separated by the electric field. This process leads to a self-enhanced type of propagation where the field in front of the streamer is also set up by space charge effects, whereas the streamer channel itself is electrically screened. Streamers that propagate towards the anode are called negative streamers. For these streamers, the electron avalanches and the streamer move in the same direction. For positive streamers, i.e. the type that propagates towards the cathode, the electrons and the streamer move in opposite directions, and a source of free electrons is required in front of the streamer head. In air, these are provided through impact excitation of molecular nitrogen, followed by spontaneous emission

and photoionisation of molecular oxygen. When a streamer bridges an electrode gap, electrical breakdown may follow if conditions for secondary discharge phenomena are met [11, 12]. For a more thorough review of streamer discharges, see e.g. [13].

1.2. Streamer–dielectric interaction

Dielectric surfaces affect streamer development in various ways, and streamers that propagate along dielectric surfaces are markedly different from bulk streamers. For example, streamers typically move faster along a dielectric surface than in the surrounding gas [14–17]. Positive streamers form a sheath with a high electric field over the surface [17–19]. Furthermore, polarisation of the dielectric can result in streamer attraction towards the dielectric surface [17, 20]. Streamers can also be influenced by the emission of secondary electrons from the dielectric surface, and by charge attachment at the surface. There are many applications that involve electrical discharges and dielectric surfaces, e.g. high voltage insulation [21, 22], dielectric barrier discharge (DBD) systems [5, 23–31], packed bed reactors [4, 8, 10, 32], and plasma medicine [33].

1.3. Streamer propagation and dielectric surface geometry

The shape, orientation and profile or roughness of a dielectric surface are all important factors for streamer propagation. Different geometries result in different propagation behaviour. In DBD geometries, the streamers typically propagate closely along the surface [18]. In arrangements with a cylindrical insulator, on the other hand, both streamer attraction and electrostatic self-repulsion have been reported [34]. Pritchard and Allen [35] found that streamers propagating along dielectrics with various high voltage insulator shed designs required higher background electric field strengths to sustain propagation than streamers along plain insulators. Chvyreva *et al* [36] showed that a dielectric surface roughness of 0.7–1 mm had little effect on electrodeless streamer inception.

To our knowledge, little attention has been devoted to streamer propagation in air over rough dielectric surfaces, or over engineered streamer-scale surface profiles. In this paper, we report on an experimental and theoretical study of positive streamer discharges over an intentionally profiled dielectric surface with 500 μm deep corrugations. We expect that this surface profile will affect streamer propagation, as the streamer thickness is around a few 100 μm in atmospheric air. The streamer velocity and range along the surface are analysed with high-speed imaging experiments and computer simulations. The experiments and simulations are performed at two voltage levels which have been selected to allow both gap-bridging streamers and arrested streamers. Both experiments and simulations are compared with a smooth surface reference geometry. Our aim is to understand how surface streamer propagation is affected by a dielectric surface profile.

The outline of this paper is as follows: in section 2 we describe the experimental setup and analysis. The simulation method is briefly presented in section 3 and we provide an experimental and theoretical analysis in section 4. The paper is concluded in section 5.
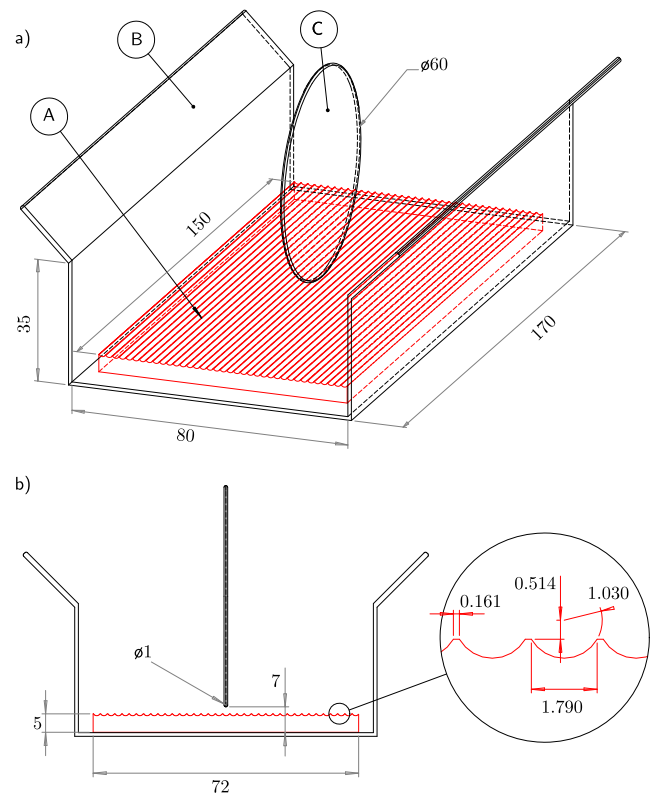
Figure 1. Setup for imaging streamers along dielectric surfaces. (a) Setup viewed from an angle, showing the profiled polycarbonate surface with 0.5 mm corrugations outlined in red (A), the grounded aluminium casing (B), and the high voltage disk electrode (C). (b) Setup viewed from the camera viewing angle, with details showing dimensions of the surface profile. All indicated dimensions are given in millimeters.
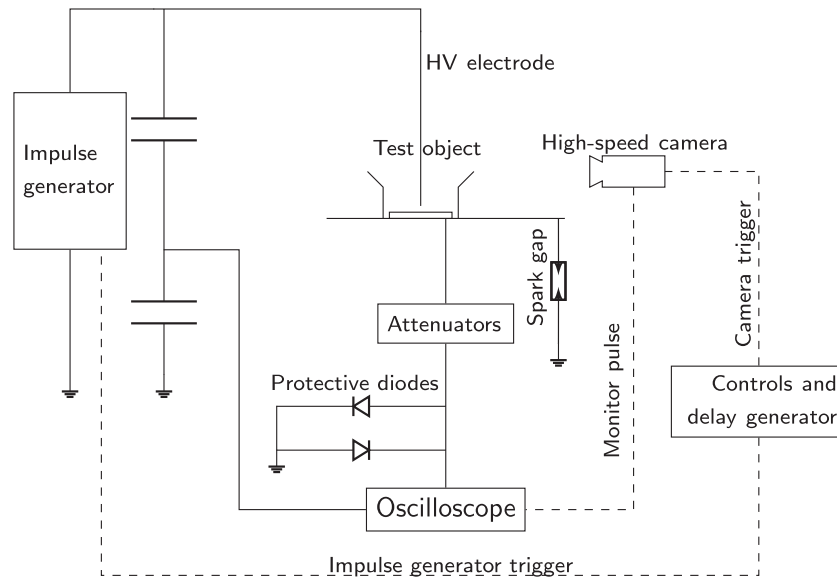
2. Experiments

In this section, the experimental setup and procedure for high-speed imaging of streamers along dielectric surfaces is presented.

2.1. Experimental setup

Figure 1 illustrates the experimental setup, including dimensions of the electrodes and the surface profile details. The setup is designed to imitate 2D planar field conditions in order to allow a comparison with computer simulations. This will be discussed in more detail in section 3.

Two polycarbonate (Lexan) slab dielectrics of 5 × 72 × 150 mm were used as test objects. In one of the dielectric slabs, a surface profile with 0.5 mm deep corrugations was drilled using a 2.4 mm diameter bore head. An aluminium casing and a disk-shaped brass electrode were used as electrodes. The disk shape was used as its electrical field distribution resembles the 2D planar simulation field, and as it provides a small streamer inception region, which facilitates imaging.

The dimensions of the profiled surface were measured with a Bruker ContourGTK profilometer and averaged. The actual corrugation depth varied between 0.487 and 0.543 mm, with an average value of 0.516 mm. When seen from the front (figure 1(b)), the average profile is outlined by 1.030 mm

Figure 2. Experimental setup. 14 or 35 kV impulses were applied to the test object in figure 1. Broken lines indicate fibre optic links.
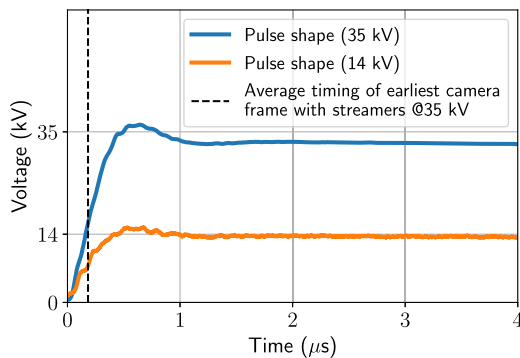
Figure 3. The applied 35 and 14 kV voltage pulse shapes in the experiments have 420 ns rise-times, and some overshoot. The average timing of the earliest streamer-illuminated camera frames at 35 kV is shown. The streamers propagate during the rising voltage flank.

radius, 120° circle sectors separated by 0.161 mm flat peaks. When using these averaged measured profile values, the profiled dielectric surface area is 1.47 times larger than a smooth surface. In other words, a streamer that perfectly sticks to the surface and propagates towards the ground wall follows a path that is approximately 50% longer than streamers propagating along the smooth surface.

2.2. Voltage pulse source

A voltage step pulse of 14 or 35 kV with 420 ns rise-time and 50 μs half-value time was applied to the disk electrode in figure 1 using a Marx impulse generator, see figures 2 and 3. The test object was grounded through a 1 × 1 m steel plane and a 50 Ω coaxial cable with overvoltage protection (a spark gap, attenuators and a diode bridge) leading to the oscilloscope to measure current. The current measurement was intended for discharge detection purposes, but it proved difficult to use as there were large oscillations in the measurement circuit during the impulse front (similar problems were reported in [37]).

The applied voltage was measured with a capacitive divider. The two applied voltage levels were selected in order to arrest the streamer on the surface (14 kV) or allow it to bridge the gap between the electrodes (35 kV).

2.3. High-speed imaging

ICCD framing cameras (Specialised Imaging SIMX and Imacon 468) were used to image streamer propagation along the dielectric surface. At 35 kV, the exposure time of each camera frame was varied between 3 and 10 ns with the SIMX camera. The SIMX camera splits the light in a total of 16 channels. One channel was malfunctioning, so a total of 15 frames were taken for each applied impulse with the SIMX. The frames were occasionally overlapped to increase the effective framerate up to 500 million frames per second. At 14 kV, a single frame with an 8000 ns exposure time was taken for each impulse with the Imacon camera.

The camera viewing angle was from the front as shown in figure 1(b). The camera focus plane was set to the part of the disk electrode closest to the dielectric surface. The images were post-processed in order to improve the visual clarity of the streamer advancement. Furthermore, the frames in each frame sequence were overlaid in order to show the accumulated light emitted by the streamer. A background image with no light was subtracted in order to normalise the light intensities. An illuminated background picture of the geometry was also overlaid in all images to illustrate the experimental setup. See section 4 for example images (figures 5 and 6).

2.4. Experimental procedure

In order to remove the residual surface charge after an impulse, a grounded rod was guided along the surface between each impulse. The camera trigger signal relative to the impulse trigger signal was controlled with a delay generator through an optical fibre. The approximate timing of the image frames relative to the impulse was monitored with a camera monitor

pulse (see figure 2). The monitor pulse timing was corrected for unequal signal propagation times in the voltage measurement and camera fibre link. The discharge initiation was regular, with a variation of a few tens of ns. It can be seen from figure 3 that the first streamer-illuminated camera frames in the 35 kV experiments occurred during the rising voltage flank. From the timing of these frames relative to the applied 35 kV voltage pulse, the instantaneous voltage at streamer inception was estimated to vary between 14 kV and 19 kV.

2.5. Estimating streamer propagation distance

The streamer horizontal propagation distance in each individual frame was estimated visually from the images. Length calculation functionality in the SIMX camera software was used. Example images are shown in section 4 (figures 5 and 6). Note that the actual streamers may also extend in the camera axis direction. Propagation in the camera axis direction is not documented here, as the images were taken only from the front. In order to locate streamer inception in time, only image series that began with an empty frame were used in the analysis. Therefore, the temporal uncertainty of the discharge inception in a frame sequence is equal to the effective frame duration, which was varied between 2 ns and 10 ns.

2.6. Data points and expected streamer range

A total of 28 image series (14 series for the profiled and 14 for the smooth surface) were taken with the SIMX camera for the 35 kV experiments, i.e. a total of 420 individual frames. Depending on the streamer velocity and inception timing, each image series had between 3 and 15 individual frames showing streamer activity. In total, there were 367 individual frames showing streamer activity (214 frames for the profiled and 153 frames for the smooth surface). At 35 kV, streamer activity was observed during every applied voltage pulse, but electrical breakdown occurred only once. Whenever there were sufficient camera frames to capture the entire streamer propagation at 35 kV, it was clear that the streamer did not stop before reaching the grounded wall.

At 14 kV, only one accumulated image, taken with the Imacon 468 camera, with 8000 ns exposure time was analysed for each surface. The 14 kV voltage level was chosen based on engineering rules for streamer propagation and inception [38]. According to these rules, the minimum external average electric field for sustained positive streamer propagation is $E_s \approx 0.5$ kV mm^{-1} in air, where E_s is called the stability field. The maximum streamer propagation range can then be estimated as the ratio of the applied voltage to the stability field. Applied to our experiments, the estimated maximum range is 28 mm at 14 kV, which is shorter than the gap between the disk electrode and the grounded wall. Moreover, the minimum streamer inception voltage of the setup was estimated at 10 kV. It was therefore expected that a 14 kV pulse would be sufficient for streamer inception, but insufficient for streamer gap crossing. However, it should be noted that the stability field estimate is an engineering simplification with limited validity, derived mainly from investigations in uniform fields. The stability field is affected by electrical field uniformity,

voltage shape, degree of streamer branching, and dielectric surface shape [35, 39–41].

3. Computer simulations

In this section, the 2D planar computer simulation model is presented. A drift–diffusion-reaction model for charge transport was used. Such models are widely used for streamer simulation in air [6, 18, 42–46]. A Helmholtz-based radiative transfer model was used to model photoionisation and photoemission.

3.1. Simulation model equations

The simulation model is formulated with the following equations:

$$\frac{\partial n}{\partial t} = -\nabla \cdot (\boldsymbol{v}n) + \nabla \cdot (D\nabla n) + S, \tag{1}$$

$$\frac{\partial \sigma}{\partial t} = J_\sigma, \tag{2}$$

$$\nabla \cdot (\epsilon_r \mathbf{E}) = \frac{\rho}{\epsilon_0}, \tag{3}$$

$$\alpha \Psi - \nabla \cdot \left(\frac{1}{3\alpha} \nabla \Psi \right) = \frac{\eta}{c}. \tag{4}$$

Equation (1) models the drift, diffusion, and plasma chemistry of charged particles. Here, n indicates the particle number density. Source terms S and transport coefficients $\boldsymbol{v}$, D were taken from Morrow and Lowke [43]. Equation (2) enforces charge balance on the dielectric surface by relating surface charge density σ to the net current density J_σ into the surface. The conductivity time constants through or along dielectrics are far greater than the streamer time scales, so solid state charge transport is disregarded in the model. Equation (3) is the Poisson equation for the electric field (**E**) where ρ is the free charge density, ϵ_0 is the vacuum permittivity, and $\epsilon_r = 3$ is the relative permittivity of the dielectric. Note that the Poisson equation is subject to a jump condition on the dielectric surface where σ appears. Equation (4) models emission of radiation using the Eddington and three-group approximations as outlined in [47]. Here, Ψ is the isotropic radiative density, α is the Beer's length, c is the vacuum speed of light and η is a photon source term. For comparison with images, the location with highest η was used as an estimate of the simulated streamer head position. Expressions for the various parameters in (1) and (4) can be found in [43, 47, 48].

3.2. Initial conditions, boundary conditions, and simulation domain

A charge-neutral uniform density of positive ions and electrons, 10^{10} m^{-3}, which is a typical level inside buildings [49], was applied as a simplified initial condition (same approach as in [42, 44, 50]). The streamer initiated in less than 1 ns in the simulations. Outflux boundary conditions were used for the charged species, and homogeneous Robin boundary conditions were used for the photon flux (see [48] for details).
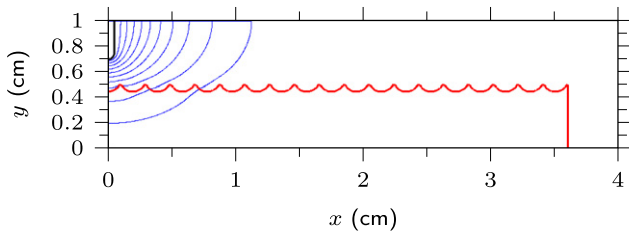
Figure 4. The figure shows the simulation domain with the high voltage electrode in black, the profiled dielectric surface in red, and background field equipotential lines in blue.

Figure 4 illustrates the simulation geometry and initial equipotential lines. Homogeneous Neumann electrical boundary conditions were placed on the left and top side of the domain in figure 4, whereas the bottom and right-hand side were electrically grounded. The simulations were performed for applied voltages of 35 kV and 14 kV on the high voltage electrode. Note that a constant peak voltage was applied in the simulation, whereas a 420 ns rise-time pulse was applied in the experiments. To model secondary emission and photoemission, the electron influx from the dielectric surface was set to be a factor of 10^{-6} times the positive ion and radiation outflux.

3.3. Space and time discretisation

The profiled surface was implemented in the simulations using the averaged measured values (figure 1) and a rounding radius of 50 μm on all corners. The model equations were discretised in space on regular Cartesian grids, with an embedded boundary formalism for describing the material boundaries, see [48] for details. The approach was combined with adaptive mesh refinement in order to limit the total grid size. A coarse grid of 1024×256 cells was used, with three additional refinement levels for the 40×10 mm domain in figure 4. The refinement ratio between the three coarsest levels was 4, and 2 between the finest, which resulted in a coarsest grid resolution of 39 μm and a minimum grid size of 1.2 μm.

The time steps Δt were primarily controlled with the Courant–Friedrichs–Lewy (CFL) condition,

$$\Delta t \leqslant k_{\mathrm{CFL}} \frac{\Delta x}{|v_x| + |v_y|}, \tag{5}$$

where $\boldsymbol{v} = (v_x, v_y)$ is the maximum species velocity in the computational cell, and $k_{\mathrm{CFL}} = 0.8$. The final time step was then also restricted by the dielectric relaxation time, see [51] for details.

3.4. Electric field conditions in simulations versus experiments

The experimental setup (figure 1) was designed to have similar background field conditions as the 2D simulations (figure 4). A larger simulation domain of 40×20 mm would have yielded a more equal background field in experiment and simulation. However, tests with a 40×20 mm domain produced similar streamer travel curves as a 40×10 mm domain, so the 40×10 mm simulation domain in figure 4 was considered adequate for the scope of this work. The constant simulation

voltages 35 and 14 kV represent upper extremities of possible instantaneous voltages for streamer propagation in the corresponding experiments.

Another important point is that the actual streamers in the experiments are 3D filamentary branches, whereas the simulated streamers are planar ionisation waves. This fundamental difference between the experiments and our model will be discussed in more detail in section 4.

4. Results and discussions

In this section, the effect of the surface profile on streamer velocity and range will be shown and discussed in the light of the results.

4.1. Visualization of discharge development

To visualize the streamer development from inception to ground, an example image series and simulations at 35 kV are shown in figures 5 and 6 for a smooth and a profiled surface respectively. In the figures, simulation plots are shown together with high-speed images at equal time instants. While the images show the accumulated streamer light emission, the simulated streamers are illustrated with electron density levels.

In both simulations and experiments, the discharge develops in the same way. A streamer initiates from the blade tip, propagates vertically, and hits the dielectric. It then propagates away from the high voltage electrode while closely following the dielectric surface. Finally, the streamer detaches from the surface and propagates over the air gap to the grounded wall.

In figure 5, both the simulated and experimental streamers reach the grounded wall within 20 ns. In figure 6 the simulated streamer reaches the ground wall in 30 ns, while the imaged streamers have only propagated around 75% of the distance from high voltage to ground after 30 ns.

4.2. Streamer velocity and travel curves

The streamer velocity depends on the intensity of the ionization mechanisms that drive the streamer forward. Higher applied field strengths imply stronger ionization and faster streamers. The influence of the background field strength on streamer propagations was clearly observed in the simulations, as the streamers would cross the gap at 35 kV, but not at 14 kV.

In figure 7, the 35 kV streamer progress along the dielectric surface in both the experiments and simulations is shown. Only one example experimental travel curve is plotted for the smooth and profiled surface respectively in figure 7 to avoid clutter. All the 28 experimental travel curves lie within the orange and blue shaded regions for the smooth and profiled surface respectively. It can be seen that streamers take a longer time to propagate from high voltage to ground along a profiled surface than along a smooth surface. This effect is seen in both experiments and simulations.

In figure 8, the horizontal distances in the profiled surface results have been multiplied by 1.47 to reflect the added area of the surface profile. The smooth and profiled surface travel curves in figure 8 are, unlike the ones in figure 7, largely
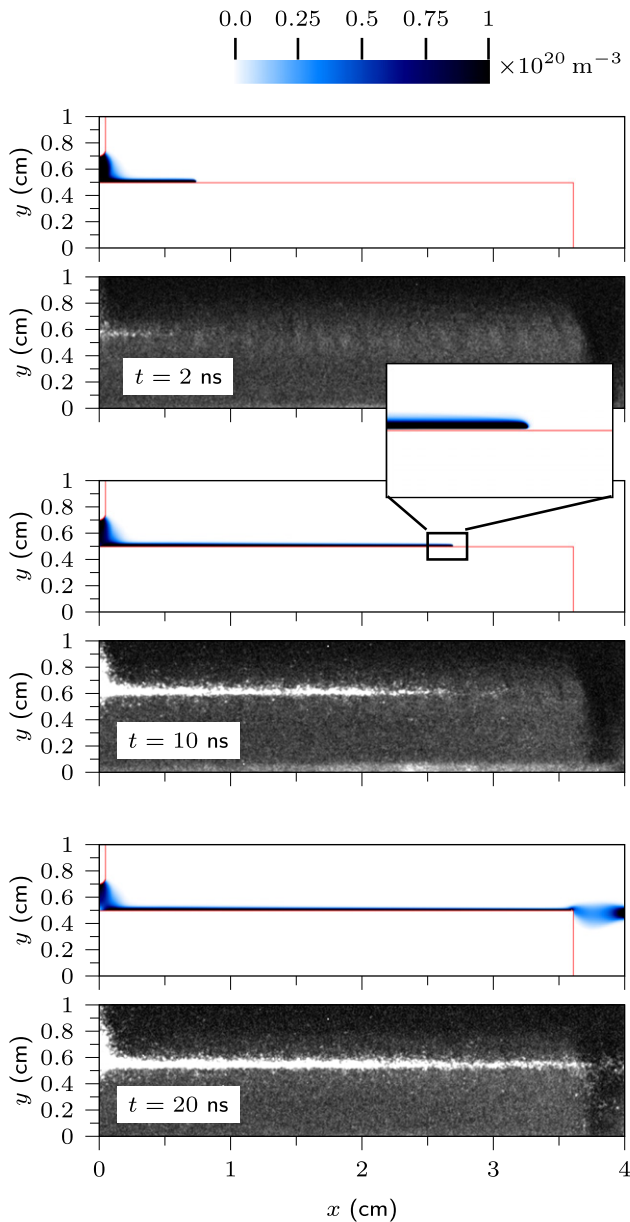
Figure 5. Streamer development along a smooth dielectric surface in experiments and simulations after 2, 10 and 20 ns. Simulation plots and images are shown together at the three different time instants. The simulated electron density is plotted to illustrate the streamer position in simulations. The inset image shows the simulated streamer front at $t = 10$ ns.
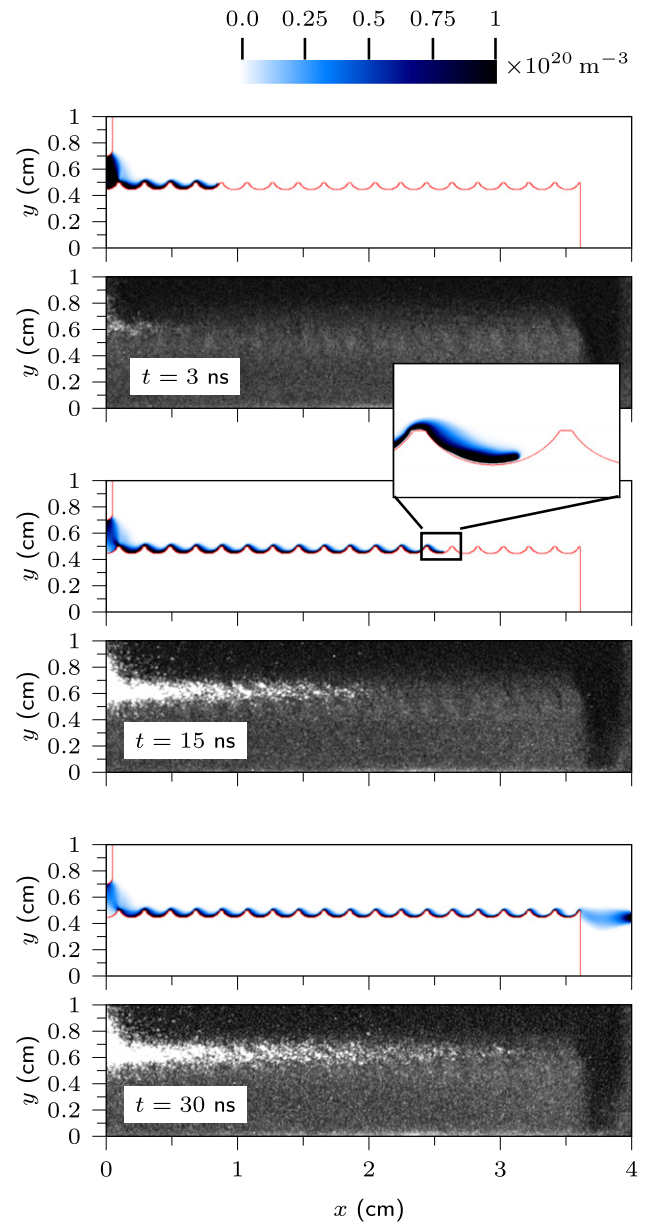
Figure 6. Streamer development along a profiled dielectric surface in experiments and simulations after 3, 15 and 30 ns. Simulation plots and images are shown together at the three different time instants. The simulated electron density is plotted to illustrate the streamer position in simulations. The inset image shows the simulated streamer front at $t = 15$ ns.

overlapping. The difference in apparent streamer velocity between the two surface types in figure 7 is therefore likely caused by differences in dielectric surface area.

The experimental data in figures 7 and 8 shows scatter on the order of 10 ns, which can largely be explained by the following effects:

(a) The streamer inception voltage varies depending on when the initial electron appears.

(b) Streamer paths are never equal in experiments, as streamers branch stochastically. Streamer path variations from one experiment to the next may result in different net streamer velocity in the horizontal direction.

(c) Small variations in residual surface charge levels from one experiment to the next may change local electric field conditions and influence the streamer path and velocity.

(d) The framing resolution of the camera may affect the apparent streamer travel curve. Different resolutions of 2, 3, 5 and 10 ns were used in the image series. The zero distance data points in figure 7 may therefore be off by up to 2, 3, 5 or 10 ns respectively for any of the 28 image series.

4.3. Simulation model limitations

There are several model limitations that prevent direct comparison of these simulations and experiments. The plasma model
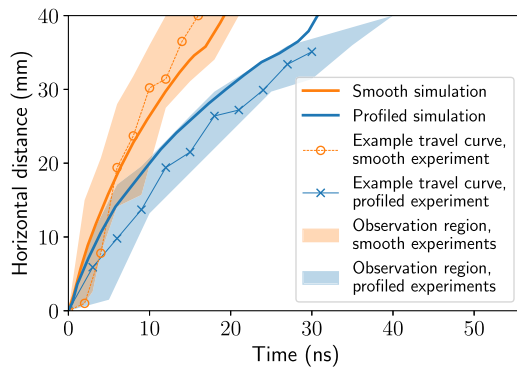
Figure 7. Travel curves of imaged and simulated streamers along a profiled and a smooth dielectric surface. The dielectric surface with 0.5 mm deep corrugations slows down streamer propagation in the horizontal direction in both simulations and experiments. Instead of showing all the 28 experimental travel curves, the regions in which all the curves lie are indicated with color shading. The two plotted example travel curves correspond to the image series shown in figures 5 and 6.
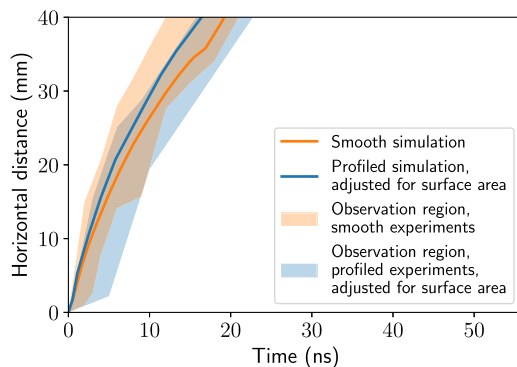
Figure 8. Travel curves of imaged and simulated streamers along a profiled and a smooth dielectric surface, corrected for surface area. The same data as in figure 7 is shown in this figure, but the horizontal distances along the profiled surface have been multiplied with 1.47, which reflects the added surface area of the corrugations.

and photoionization model simplify the ionization mechanisms greatly. The greatest limitation, however, is the missing third dimension in the simulation model. While real streamers are three-dimensional branching filaments, the modeled streamer is a planar ionization wave. Note that using axisymmetric setups would not help since a radially propagating streamer would resemble a planar ionization wave for large radii. For a given applied voltage, a 3D streamer filament experiences a more inhomogeneous, strong field at its front than a planar streamer does. The stronger field at the front suggests that a 3D streamer is ordinarily faster than a 2D planar streamer. To verify this, we compared the 2D axi-symmetrical reference case 3 in [44] with a corresponding 2D planar simulation in our model. The r, z dimensions in the reference case 3 in [44] were simply replaced with Cartesian x, y dimensions, while all the other physical parameters in the simulations were kept equal. The resulting 2D planar streamer was, as expected, much slower, having propagated less than a millimeter in 40 ns,

whereas the axisymmetrical streamers in [44] propagate around 1 mm ns^{-1}.

Another important limitation of the simulations is the omission of the voltage rise-time. In the 35 kV experiments, the streamers propagate during the rising flank of the pulse, and experience an instantaneous voltage at inception between 14 and 19 kV, see figure 3. The simulated streamers should therefore propagate faster than the experimental streamers, since there is a full 35 kV applied potential in the model. However, as can be seen from figure 7, the simulated streamers are not generally faster than the experimental streamers. These discrepancies probably result from the two-dimensional simplification of the computer model as discussed above. In summary, the two-dimensional simplification makes the simulated streamer slower than the experimental streamer, while the constant voltage simplification makes it faster. Both simplifications are important limitations of our model.

4.4. Surface profile effect

Although exact agreement between experiments and simulations could not be reached, it is clear that streamers propagating along the profiled surface take a longer time to reach the ground electrode. This effect is evident in both simulations and experiments. Arguably, the surface profile effect is fundamentally the same in both experiments and simulation. If the streamers follow the surface profile closely, longer streamers are required to traverse a profiled than a smooth surface. As the voltage drop along a streamer increases with the streamer length, a streamer extension leads to a reduction of the residual voltage at the streamer front. When the residual voltage at the streamer front is reduced, there is less energy available at the front to drive ionization. Consequently, the streamer advancement towards the ground electrode is slowed down along the profiled surface.

In addition to the streamer-extending effect of the surface profile, the streamer may be further inhibited by the way in which the profile deflects the streamer locally. In figure 9, the electric field strength is plotted as a streamer front propagates over a profile corrugation. Note that since the simulation output was only plotted for every hundredth time-step, the time step between plots in figure 9 is unequal (the time step was varied according to (5)). In the first six plots in figure 9, the streamer is climbing (i.e., propagating in positive y-direction) out of a corrugation. In the next three plots, the streamer is descending into the following corrugation. The streamer decelerates when climbing, and accelerates when descending. As a result, the streamer uses around 0.4 ns to climb the corrugation in figure 9, and only 0.3 ns to descend it. Propagation from one corrugation floor to the next took 0.9 ns (from 2.67 ns to 3.58 ns). The changing streamer velocity in figure 9 is a result of changing electric and geometric conditions. As the streamer climbs a corrugation in figure 9, the surface profile forces it to propagate away from the cathode. Moreover, the dielectric peak physically obstructs the ionisation processes to a larger degree when the streamer is climbing. Electrons can be recruited from a larger volume when the streamer is
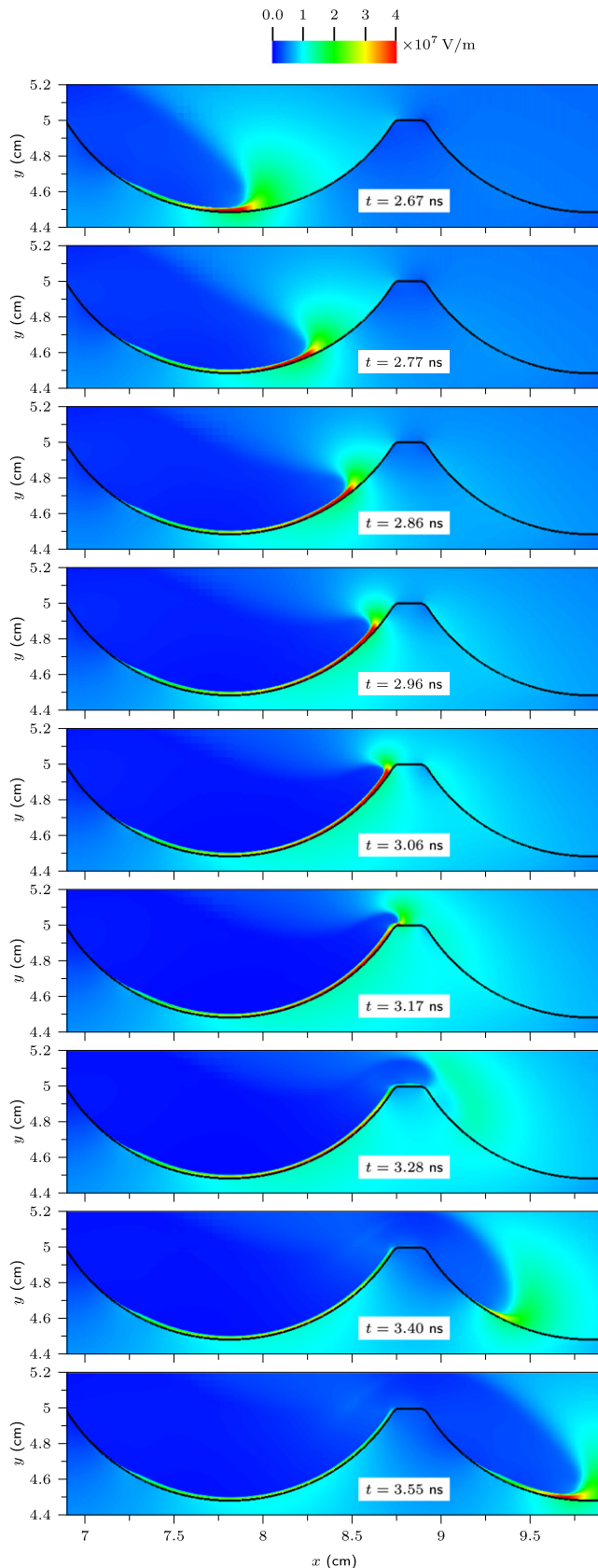
Figure 9. Electric field strength plots at different time instants (from $t = 2.67$ ns to $t = 3.55$ ns) of streamer propagation over a profile corrugation, 35 kV applied.

Table 1. Streamer stopping length in simulations and experiments at 14 kV (numbers in mm).

	Smooth surface	Profiled surface
Experiments	28	14
Simulations	34.9	16.4

descending, and the electron avalanches that advance the streamer are less obstructed by the solid dielectric.

4.5. Streamer range

At 14 kV, the 8000 ns camera frames showed that the streamers did not make it to the ground wall, whereas the streamer crossed the electrode gap at 35 kV (figure 7). The streamer was also arrested in the corresponding 14 kV simulations. The profiled 14 kV simulation was run for around 400 ns, with no streamer advancement in the last 300 ns, while the smooth 14 kV simulation was run for around 300 ns with no advancement in the last 150 ns. The estimated streamer propagation distances in simulations and experiments at 14 kV are presented in table 1. Figure 10 shows the evolution of the simulated electric field strength as the streamer is stopping while climbing a corrugation. Table 1 shows that streamers propagate around twice as long along a smooth surface as along a profiled surface in both simulations and experiments at 14 kV.

A typical engineering rule for estimating streamer range in ambient air was discussed in section 2. The rule assumes that the positive streamer channel needs a minimum average background field strength of around 0.5 kV mm^{-1} in air to sustain propagation [15]. This field is called the stability field E_s. The streamer range s_r can then be expressed as

$$s_r = U/E_s, \qquad (6)$$

where U is the applied voltage. As discussed earlier, the profiled surface increases the streamer length since the streamer propagates closely along the surface. As the profiled surface is 47% longer than the smooth surface, it is expected that the horizontal streamer range along the profiled surface s_{xr} is around

$$s_{xr} = U/E_s \cdot \frac{1}{1.47}. \qquad (7)$$

However, results from both experiments and simulations in table 1 indicate that s_{xr} is around

$$s_{xr} = U/E_s \cdot \frac{1}{2}. \qquad (8)$$

In simulations, the streamer stopped while climbing out of a corrugation. The additional decelerating effects of propagating out a corrugation that were discussed in section 4.4 may inhibit the streamer additionally and possibly explain the lower s_{xr}.

However, the experimental data is limited for the 14 kV tests, with only one data point for each surface type. Moreover, the streamer was faint at 14 kV and the imaging resolution was rather low, so the exact streamer position was
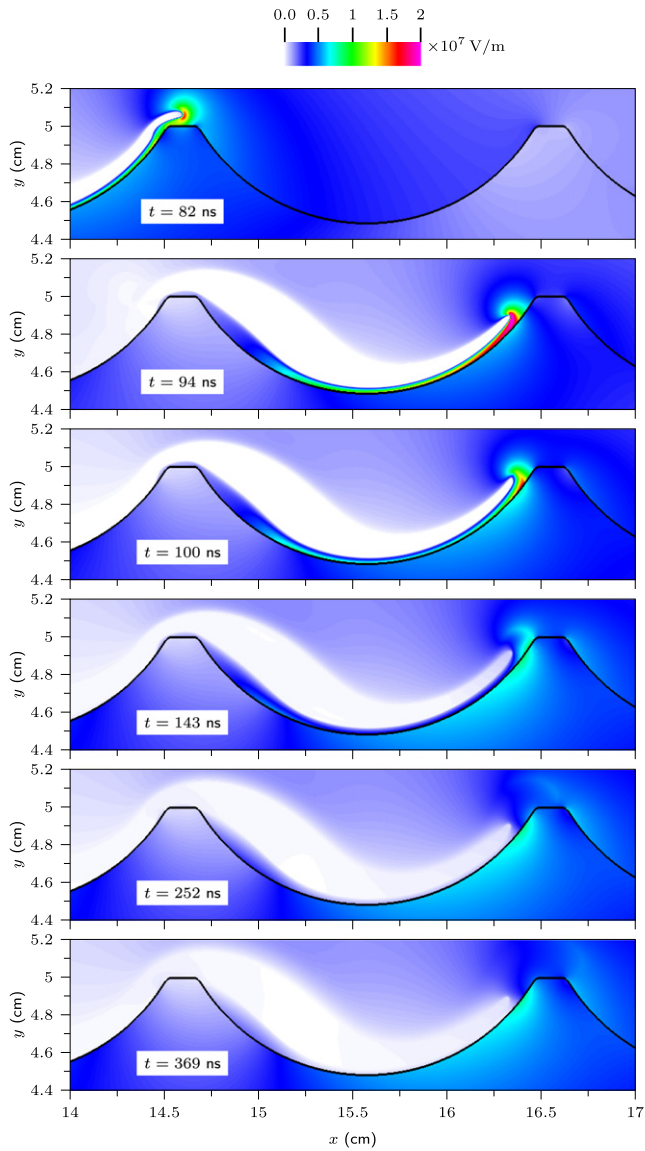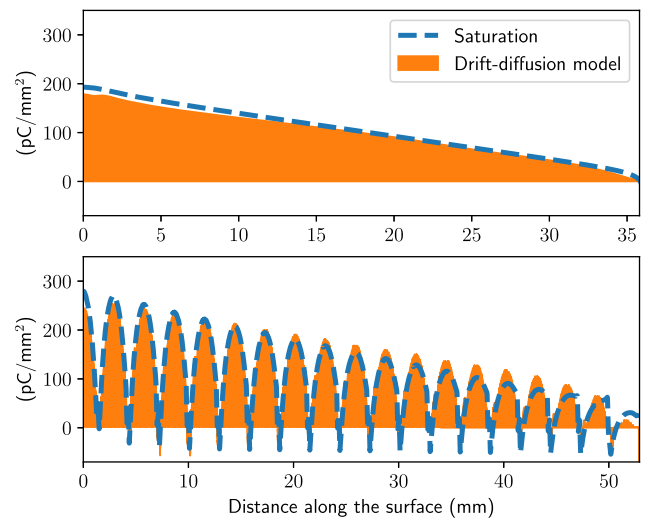
Figure 10. Electric field strength plots at different time instants (from $t = 82$ ns to $t = 369$ ns) of streamer propagation, 14 kV applied. The streamer is stopping while climbing a corrugation at around $x = 16.4$ mm.

Figure 11. The resulting simulated surface charge distributions along the smooth surface (top plot) and the profiled surface (bottom plot) approach saturation charge.

difficult to estimate correctly. Nevertheless, both experiments and simulations demonstrate that the profiled surface limits the range of streamers propagating along it.

4.6. Streamer surface charging

Dielectric surface charging effects may impact the streamer propagation dynamics.

With both surface types, the simulated surface charge distributions after streamer propagation are close to the defined saturation charge [19, 38]. This is illustrated in figure 11. The saturation charge condition implies that the space-charge free electric field at the air-side of the dielectric–air boundary is zeroed by surface charges at the boundary. With saturation conditions, the surface charge intensity is highest down in the corrugations for the profiled surface, whilst it transitions continuously from a high to a low level along the smooth surface.

Moreover, some negative charge accumulates on the corrugation slopes that are not facing the electrode. The electrostatic saturation charge distributions in figure 11 were calculated with commercial finite element method software. The drift–diffusion simulation time instants in figure 11 are 38 and 31 ns for the smooth and the profiled surface respectively, with 35 kV applied.

In previous work by some of the authors [19], it was shown that streamer surface charging in our drift–diffusion model is dominated by ion drift from the streamer filament, rather than by ionisation processes near the streamer head. It can therefore be argued that surface charging effects do not strongly govern the streamer propagation velocity and range, assuming that the surface is charge-neutral to begin with. The streamer velocity and range are mainly determined by the ionisation processes near the streamer head.

5. Conclusion

We have investigated positive streamer propagation along a profiled and a smooth dielectric surface using high-speed image experiments and 2D planar drift–diffusion simulations. The surface profile consisted of linear corrugations of 0.5 mm depth. The streamers take a longer time to reach the ground electrode when the profiled surface is used. When arrested, streamers propagating along the profiled surface have a shorter range. These effects were observed in both experiments and simulations.

The surface profile effect can largely be explained in terms of the increased streamer propagation length along a profiled surface, but the streamer is also inhibited by changing geometric and electrical conditions along the profiled surface. Quantitative agreement between simulations and experiments was not achievable, as the voltage pulse shape and streamer 3D effects were not included in the computer model. Nevertheless, the results provide insights in the dynamics of streamer propagation along a profiled dielectric surface, both from an

experimental and a theoretical point of view. They also demonstrate the inaccuracy of engineering estimates of streamer ranges.

Understanding the nature of streamer–dielectric interaction is of importance for various applications, e.g. in high voltage engineering, aerodynamic flow control, plasma medicine and lightning research. For high-voltage applications, surface profiles as the one used here can possibly inhibit streamers without compromising on the mechanical strength or volume of the insulator.

Acknowledgments

ORCID iDs

H K H Meyer https://orcid.org/0000-0002-9436-6518
R Marskar https://orcid.org/0000-0003-1706-9736
F Mauseth https://orcid.org/0000-0003-3795-0205

References

[1] Fullekrug M, Mareev E A and Rycroft M J 2006 *Environ. Sci.* (New York: Springer) **225** 398

[2] Dinelli G, Civitano L and Rea M 1990 *IEEE Trans. Ind. Appl.* **26** 535

[3] Clements J S, Mizuno A, Finney W C and Davis R H 1989 *IEEE Trans. Ind. Appl.* **25** 62

[4] Van Laer K and Bogaerts A 2015 *Energy Technol.* **3** 1038–44

[5] Boeuf J P and Pitchford L C 2005 *J. Appl. Phys.* **97** 103307

[6] Soloviev V R and Krivtsov V M 2009 *J. Phys. D: Appl. Phys.* **42** 125208

[7] Soloviev V and Krivtsov V 2017 *J. Phys.: Conf. Ser.* **927** 012059

[8] Van Laer K and Bogaerts A 2015 *Plasma Sources Sci. Technol.* **25** 015002

[9] Zhang Q-Z and Bogaerts A 2018 *Plasma Sources Sci. Technol.* **27** 035009

[10] Wang W, Kim H H, Van Laer K and Bogaerts A 2018 *Chem. Eng. J.* **334** 2467–79

[11] Seeger M, Votteler T, Ekeberg J, Pancheshnyi S and Sanchez L 2018 *IEEE Trans. Dielectr. Electr. Insul.* **25** 2147

[12] Kojima H, Hotta K, Kitamura T, Hayakawa N, Otake A, Kobayashi K, Kato T, Rokunohe T and Okubo H 2016 *IEEE Trans. Dielectr. Electr. Insul.* **23** 194

[13] Ebert U, Montijn C, Briels T M P, Hundsdorfer W, Meulenbroek B, Rocco A and Veldhuizen E M v 2006 *Plasma Sources Sci. Technol.* **15** S118

[14] Allen N L and Mikropoulos P N 1999 *IEEE Trans. Dielectr. Electr. Insul.* **6** 357

[15] Allen N L and Mikropoulos P N 2001 *IEEE Trans. Dielectr. Electr. Insul.* **8** 812

[16] Sobota A, Lebouvier A, Kramer N J, van Veldhuizen E M, Stoffels W W, Manders F and Haverlag M 2008 *J. Phys. D: Appl. Phys.* **42** 015211 Publisher: IOP Publishing

[17] Li X, Sun A, Zhang G-J and Teunissen J 2020 *Plasma Sources Sci. Technol.* **20** 065004

[18] Soloviev V R and Krivtsov V M 2014 *Plasma Phys. Rep.* **40** 65

[19] Meyer H K, Mauseth F, Marskar R, Pedersen A and Blaszczyk A 2019 *IEEE Trans. Dielectr. Electr. Insul.* **26** 1163

[20] Li X, Sun A and Teunissen J 2020 *IEEE Trans. Dielectr. Electr. Insul.* **27** 1178

[21] Roser H 1932 *Elektrotech. Z.* **H17** pp 411–2

[22] Lebedev S M, Gefle O S and Pokholkov Y P 2005 *IEEE Trans. Dielectr. Electr. Insul.* **12** 537

[23] Kogelschatz U 2003 Dielectric-barrier discharges: their history, discharge physics, and industrial applications (arXiv:0005074v1 [arXiv:astro-ph])

[24] Moreau E 2007 *J. Phys. D: Appl. Phys.* **40** 605

[25] Jayaraman B, Cho Y C and Shyy W 2008 *J. Appl. Phys.* **103** 053304

[26] Likhanskii A V, Shneider M N, Macheret S O and Miles R B 2008 *J. Appl. Phys.* **103** 053305

[27] Celestin S, Bonaventura Z, Guaitella O, Rousseau A and Bourdon A 2009 *Eur. Phys. J. Appl. Phys.* **47** 22810

[28] Corke T C, Enloe C L and Wilkinson S P 2010 *Annu. Rev. Fluid Mech.* **42** 505–29

[29] Pechereau F, Bonaventura Z and Bourdon A 2016 *Plasma Sources Sci. Technol.* **25** 044004

[30] Gibalov V I and Pietsch G J 2000 *J. Phys. D: Appl. Phys.* **33** 2618 publisher: IOP Publishing

[31] Wollny A *et al* 2011 *Appl. Phys. Lett.* **99** 141504

[32] Russ H, Neiger M and Lang J E 1999 *IEEE Trans. Plasma Sci.* **27** 38

[33] Laroussi M 2018 *Plasma* **1** 47

[34] Dubinova A A 2016 Modeling of streamer discharges near dielectrics *PhD Thesis* Eindhoven: TU Eindhoven oCLC: 956923350

[35] Pritchard L S and Allen N L 2002 *IEEE Trans. Dielectr. Electr. Insul.* **9** 371

[36] Chvyreva A, Pancheshnyi S, Christen T and Pemen A J M 2018 *J. Phys. D: Appl. Phys.* **51** 115202 publisher: IOP Publishing

[37] Nijdam S 2011 Experimental investigations on the physics of streamers *PhD Thesis* TU Eindhoven

[38] Pedersen A and Blaszczyk A 2017 *IEEE Trans. Dielectr. Electr. Insul.* **24** 2775

[39] Allen N L and Ghaffar A 1995 *J. Phys. D: Appl. Phys.* **28** 331 publisher: IOP Publishing

[40] Babaeva N Y and Naidis G V 1996 *Phys. Lett.* A **215** 187

[41] Babaeva N Y and Naidis G V 1997 *IEEE Trans. Plasma Sci.* **25** 375

[42] Viegas P, Slikboer E, Obrusník A, Bonaventura Z, Sobota A, Garcia-Caurel E, Guaitella O and Bourdon A 2018 *Plasma Sources Sci. Technol.* **27** 094002

[43] Morrow R and Lowke J J 1997 *J. Phys. D: Appl. Phys.* **30** 614

[44] Bagheri B *et al* 2018 *Plasma Sources Sci. Technol.* **27** 095002

[45] Babaeva N Y, Naidis G V and Kushner M J 2018 *Plasma Sources Sci. Technol.* **27** 015016

[46] Singh S and Serdyuk Y V 2019 *IEEE Trans. Plasma Sci.* **47** 729

[47] Bourdon A, Pasko V P, Liu N Y, Célestin S, Ségur P and Marode E 2007 *Plasma Sources Sci. Technol.* **16** 656

[48] Marskar R 2019 *J. Comput. Phys.* **388** 624

[49] Pancheshnyi S 2005 *Plasma Sources Sci. Technol.* **14** 645

[50] Pechereau F, Jánský J and Bourdon A 2012 *Plasma Sources Sci. Technol.* **21** 055011

[51] Marskar R 2020 *Plasma Sources Sci. Technol.* **29** 055007